IEEE/CSC & ESAS SUPERCONDUCTIVITY NEWS FORUM (global edition), October 2015.
Invited poster presentation 3A-LS-O1.8 given at EUCAS 2015; Lyon, France, September 6 – 10, 2015.
A manuscript was submitted to *IEEE Trans. Appl. Supercond.* for possible publication.

3D modeling and measurement of coupling AC loss in soldered tapes and striated coated conductors

E. Pardo, *Member, IEEE*, M. Kapolka, J. Kováč, J. Šouc, F. Grilli, R. Nast, A. Piqué

***Abstract*—Coupling AC loss between superconducting filaments or tapes produces additional heating, complicating the cryogenics of superconducting applications and reducing their efficiency. Predicting the coupling currents and the loss that they generate in general 3D samples require numerical computations. These may reduce the coupling loss by sample optimization and are necessary for the device design. In this work we model and measure coupling (and hysteresis) loss of soldered and striated tapes. Coupling loss is measured at 72 and 144 Hz for applied fields up to 100 mT amplitude and frequencies from 2.4 to 576 Hz for applied magnetic fields around 4 mT. Modelling is based on an original variational principle. This model is also benchmarked with Finite Element Method computations, showing good agreement. For both models, we assume an isotropic power-law relation between the electric field and current density. We also introduce a simpler 3D model that assumes zero resistivity in the superconductor. The latter model, together with cross-sectional methods for the hysteresis loss, is enough to satisfactorily predict the AC loss, except for applied field amplitudes above the loss factor peak and very short samples. The variational method is promising for more complicated 3D situations.**

***Index Terms*—Coupling AC losses, hysteresis AC losses, coated conductors, computer modelling, striations**

I. Introduction

AC loss in superconducting devices reduces the efficiency and generates heat within the cryostat, complicating the cyogenics [1]. Due to their relatively large width, coated conductors create high hysteresis loss when submitted to AC magnetic fields. This could be reduced by striations [2], [3]. However, coupling loss in the current leads or due to residual normal conductor between the filaments creates coupling loss [4], [5]. Then, transposition is necessary, either by twisting the tape [6] or by making circular cables, or Conductor On Round Core (CORC) cables [7]. In order to predict the AC loss for a given transposition length and interpret the AC loss measurements, computer modelling is necessary [1].

There are several works on modelling of striated tapes. First, the coupling currents between two superconducting filaments were calculated either by finite element methods [8] and integral methods [9]. The latter allowing to restrict the calculations to the superconductor volume. Later, coupling currents and losses were calculated with a thin film model in the $\mathbf{T}-\Omega$ formulation [6], [10], also avoiding meshing the air around the sample.

Alternatively, variational methods for 2D surfaces were introduced in [11]–[13], which do not require to mesh the air. However, the coupling problem was not analyzed. In addition, these variational methods are not suitable for general 3D problems as formulated in those articles.

This article presents a 3D variational method to calculate the superconductor response under varying magnetic fields, including the coupling situation. We also present a simpler 3D model to compute the coupling currents and loss for low applied magnetic field amplitudes, which assumes zero resistivity in the supercondutor. Both methods avoid meshing the air. In particular, this work studies striated coated conductors and soldered tapes. The latter not only serves as a simple situation similar to striations but also is interesting for multi-tape cables, such as Roebel [14] and CORC cables [15]. We also compare the calculation results with AC loss measurements, in order to evaluate the usefulness of the models.

II. Experimental method

A. Sample preparation

The soldered samples were prepared by joining 6 mm wide SuperPower tape (20 μm thick copper stabilized) with In at the edges (figure 1). Two samples were prepared by the same process, showing $\sim$15 % difference in the tape-to-tape resistance per unit length, obtained by electrical measurements. Similar deviations were found in a 1 cm piece cut from the samples, evidencing fluctuations of the resistance per unit length of the same order. The final samples were 50 mm long and presented 810 and 710 nΩ of resistance, respectively. After measuring the AC loss, the 710 nΩ sample was cut to 22 mm length for further measurements.

The 10-filament striated samples were prepared from 12 mm wide SuperPower [16] tapes by a picosecond laser [5], [17]. In this article, we analyze tapes with both $\sim$2 μm silver stabilization and additional 20 μm copper stabilization. The stabilization at the edges was removed in order to eliminate coupling effects due to the lower copper layer, as shown in figure 1. For the Cu stabilized samples, the measured filament-to-filament resistance per unit tape length is roughly the same for all filaments, with value 13.33 nΩ/m [5]. The striation groove width is of 20 μm.

B. AC loss measurement

The measurement system is based on the calibration-free method [18], which allows experimental studies of the AC

Preprint of invited poster 3A-LS-O1.8 presented at EUCAS 2015, Lyon, France, September 6–10, 2015

E. Pardo, M. Kapolka, J. Kováč, J. Šouc and A. Pique are with the Institute of Electrical Engineering, Slovak Academy of Sciences, Dubravska 9, 84104 Bratislava, Slovakia.

F. Grilli is with Karlsruhe Institute of Technology, Karlsruhe, Germany.

We acknowledge the previously-published measurement data form E. Demencik for striated tapes.

IEEE/CSC & ESAS SUPERCONDUCTIVITY NEWS FORUM (global edition), October 2015.
Invited poster presentation 3A-LS-O1.8 given at EUCAS 2015; Lyon, France, September 6 – 10, 2015.
A manuscript was submitted to *IEEE Trans. Appl. Supercond.* for possible publication.

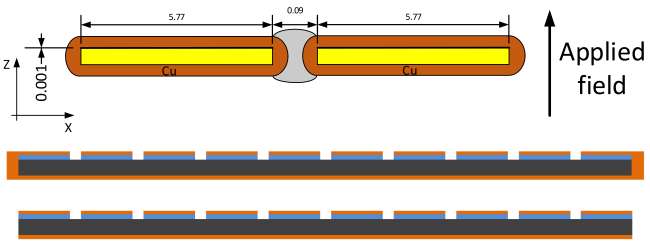

Fig. 1. Top: sketch of the cross-section of the soldered tapes, where the the yellow rectangles represent the hastelloy substrate, the thicker black line on top represents the superconductor and the gray region in between represents the solder metal. Center: sketch fo the cross-section of striated sample with copper stabilization, where orange is the copper, blue represents the silver and gray is the hastelloy (superconductor between silver and hastelloy not shown). Bottom: Striated tape with etched copper stabilization at the edges.

loss due to applied external fields of various amplitudes, frequencies and temperatures. To increase the accuracy and sensitivity of AC measurements, some modifications of original calibration free method was done [19], [20]. The present system is able to measure magnetization AC losses with high precision and sensitivity in external fields ranging from 10^{-4} T up to 10^{-1} T at frequencies between 72 Hz and 144 Hz. At lower field amplitudes (up to 18 mT) AC loss measurements can be performed in a wide frequency range, from 2.3 Hz up to 1152 Hz.

III. Models

A. Linear material model

The basic equations for both the linear material and the variational principle (sections III-A and III-B) are

$$\mathbf{E} = -\dot{\mathbf{A}} - \nabla\phi \quad (1)$$

$$\nabla \cdot \mathbf{A} = 0, \quad (2)$$

where $\mathbf{E}$ is the electric field, $\mathbf{A}$ and ϕ are the vector and scalar potentials, respectively, $\dot{\mathbf{A}}$ is the time derivative of $\mathbf{A}$ and the second equation corresponds to Coulomb's gauge. We also take the material $\mathbf{E}(\mathbf{J})$ relation into account, where $\mathbf{J}$ is the current density. For the linear material model $\mathbf{E} = \rho\mathbf{J}$, where ρ is the resistivity and we assume $\rho = 0$ in the superconductor. This assumption is valid for the limit of low applied magnetic field amplitudes only, where the superconductor experiences perfect magnetic shielding.

From equations (1) and (2), and Maxwell equations, $\mathbf{A}$ and ϕ are related to $\mathbf{J}$ and q (q is the charge density) as

$$\phi(\mathbf{r}) = \frac{1}{4\pi\epsilon_0}\int \mathrm{d}V' \frac{q(\mathbf{r}')}{|\mathbf{r}-\mathbf{r}'|} \quad (3)$$

$$\mathbf{A}(\mathbf{r}) = \mathbf{A}_s(\mathbf{r}) + \frac{1}{4\pi c^2}\int \mathrm{d}V' \frac{\dot{\mathbf{E}}(\mathbf{r}')}{|\mathbf{r}-\mathbf{r}'|}, \quad (4)$$

(5)

where

$$\mathbf{A}_s(\mathbf{r}) = \frac{\mu_0}{4\pi}\int \mathrm{d}V' \frac{\mathbf{J}(\mathbf{r}')}{|\mathbf{r}-\mathbf{r}'|} \quad (6)$$

is the vector potential for the static case, $\mathrm{d}V$ is the volume differential, ϵ_0 and μ_0 are the void permitivity and permeability, respectively, and $c = 1/\sqrt{\epsilon_0\mu_0}$ is the speed of light. The Coulomb's gauge condition is

$$\nabla \cdot \mathbf{A}_s + \dot{\phi}/c^2 = 0. \quad (7)$$

For low enough frequencies, equation (1) becomes

$$\mathbf{E} \approx -\dot{\mathbf{A}}_s + \mathbf{E}_e, \quad (8)$$

$$\mathbf{B} \approx \nabla \times \mathbf{A}_s \quad (9)$$

where we used equation (4), $\mathbf{E}_e \equiv -\nabla\phi$ is the electrostatic field and $\mathbf{B}$ is the magnetic flux density. The approximation above corresponds to dropping terms with second time derivatives, $\ddot{\mathbf{E}}$ and $\ddot{\mathbf{B}}$, which are negligible for low frequencies[1].

Although it is possible to also drop $\dot{\phi}$ in equation (7) to solve the electromagnetic problem, we keep the full equation in the numerical approach of the models in sections III-A and III-B. From vector calculus relations, it can be seen that equation (7) corresponds to

$$\nabla \cdot \mathbf{J} + \dot{q} = 0. \quad (10)$$

The computational methods of sections III-A and III-B obtain $\mathbf{J}$ and q by solving equations (8) and (7) [or (10)] for the given $\mathbf{E}(\mathbf{J})$ relation. For this purpose, $\mathbf{J}$ and q are discretized as follows. We divide the superconductor into rectangular cells (or prisms), where q is assumed uniform. The normal component of $\mathbf{J}$ to the prism surfaces is assumed uniform at the surfaces. Taking the cartesian coordinates xyz such that each edge of the prisms is parallel to one axis,

$$J_p(\mathbf{r}) = \sum_i^{n_{sp}} h_{pi}(\mathbf{r}) J_{pi}, \quad (11)$$

where $p \in \{x, y, z\}$, n_{sp} is the total number of surfaces perpendicular to the axis p and $h_{pi}(\mathbf{r})$ is the interpolation function that is 1 at the surface i of kind p, 0 at all the other surfaces and varies linearly between the neighbour surfaces of the same kind. We define the following average of the p component of $\mathbf{A}_s$, A_{sp}, at the volume of influence of surface i of kind p

$$A_{spi} = \int \mathrm{d}V h_{pi}(\mathbf{r}) A_{sp}(\mathbf{r}) = \sum_j^{n_{sp}} a_{pij} J_{pj} \quad (12)$$

where

$$a_{pij} = \frac{\mu_0}{4\pi}\int \mathrm{d}V \int \mathrm{d}V' \frac{h_{pi}(\mathbf{r}) h_{pj}(\mathbf{r}')}{|\mathbf{r}-\mathbf{r}'|}, \quad (13)$$

where we applied the discretization. Similarly, we define

$$E_{epi} = \int \mathrm{d}V h_{pi}(\mathbf{r}) E_{ep}(\mathbf{r}) = \sum_j^{n_c} e_{pij} q_j \quad (14)$$

with

$$e_{pij} = \frac{1}{4\pi\epsilon_0}\int \mathrm{d}V \int_{V_j} \mathrm{d}V' h_{pi}(\mathbf{r}) \frac{p - p'}{|\mathbf{r}-\mathbf{r}'|^3}, \quad (15)$$

where n_c is the number of cells, V_j is the volume of cell j, $p \in \{x, y, z\}$ and p' has the same form as p but with prime.

[1]The Fourier transform of $\ddot{\mathbf{E}}(t)$ is $-\omega^2\mathbf{E}(\omega)$, where t is the time, ω is the angular frequency and $\mathbf{E}(\omega)$ is the Fourier transform of $\mathbf{E}(t)$. The additional term in equation (8) is proportional to $(\omega/c)^2$, and thence much smaller than the remaining terms for low enough frequencies. The same argument applies for equation (9).

IEEE/CSC & ESAS SUPERCONDUCTIVITY NEWS FORUM (global edition), October 2015.
Invited poster presentation 3A-LS-O1.8 given at EUCAS 2015; Lyon, France, September 6 – 10, 2015.
A manuscript was submitted to *IEEE Trans. Appl. Supercond.* for possible publication.

With this discretization and taking the time Fourier transform of all electromagnetic quantities, such as $\mathbf{J}(\mathbf{r},t) = \int_{-\infty}^{\infty} \mathrm{d}\omega \mathbf{J}(\mathbf{r},\omega)e^{\imath\omega t}$ where $\imath$ is the imaginary unit, we obtain the following set of equations for linear materials

$$\sum_{j}^{n_{sp}} J_{pj}(\omega)[\rho_{pj}\delta_{ij} + \imath\omega a_{pij}] - \sum_{j}^{n_c} e_{pij} q_j(\omega) = -\imath\omega A_{ap}(\omega) \quad (16)$$

$$\imath\omega q_i(\omega) + \sum_{p\in\{x,y,z\}} \sum_{j}^{n_{sp}} D_{pij} J_{pj}(\omega) = 0, \quad (17)$$

where ρ_{pj} is the resistivity at surface j of the p kind, δ_{ij} is Kronecker's delta, A_{ap} is the p component of the vector potential due to an applied magnetic field[2], $\mathbf{B}_a = \nabla \times \mathbf{A}_a$, and D_{pij} are constant coefficients defined such that at cell i

$$[\nabla \cdot \mathbf{J}]_i = \oint_{S_i} \mathrm{d}\mathbf{S} \cdot \mathbf{J} = \sum_{p\in\{x,y,z\}} \sum_{j}^{n_{sp}} D_{pij} J_{pj}, \quad (18)$$

where S_i is the cell i surface and $\mathrm{d}\mathbf{S}$ its differential. For each angular frequency, $\mathbf{J}(\mathbf{r},\omega)$ and $q(\mathbf{r},\omega)$ is numerically found by solving the set of linear equations (16) and (17). For sinusoidal excitations in the steady state, it is enough to solve these equations for the excitation frequency.

B. Variational principle

For the variational principle, we take the same theoretical background and discretization as for the linear model [deduction up to equation (15)]. It can be seen that equation (8) for a given $\mathbf{E}(\mathbf{J})$ relation corresponds to the Euler-Lagrange equations for $\mathbf{J}$ of the following functional for a given time [21]

$$L_J = \int \mathrm{d}V \left[\frac{1}{2}\Delta\mathbf{J} \cdot \frac{\Delta\mathbf{A}_{sJ}}{\Delta t} + \Delta\mathbf{J} \cdot \frac{\Delta\mathbf{A}_a}{\Delta t} + U(\mathbf{J}) + \nabla\phi \cdot \mathbf{J} \right] \quad (19)$$

with

$$U(\mathbf{J}) = \int_0^{\mathbf{J}} \mathrm{d}\mathbf{J}' \cdot \mathbf{E}(\mathbf{J}'), \quad (20)$$

where $\Delta\mathbf{J} = \mathbf{J} - \mathbf{J}_0$ and $\mathbf{J}_0$ is the current density at the previous time step, Δt is the time step, $\Delta\mathbf{A}_{sJ}$ is the $\mathbf{A}_s$ that $\Delta\mathbf{J}$ generates, and $\Delta\mathbf{A}_a$ is the change in applied vector potential in the time step. Then, for a given ϕ (or q, which generates ϕ), $\mathbf{J}$ if found by minimizing the functional above. For a given $\mathbf{J}$, equation (7) is the Euler-Lagrange equation for q of the following functional

$$L_q = \int \mathrm{d}V \left[\frac{1}{2}\Delta q \frac{\Delta\phi}{\Delta t} - \nabla\phi \cdot \mathbf{J} \right], \quad (21)$$

where $\Delta q = q - q_0$, q_0 is the charge density at the previous time step and $\Delta\phi$ is the electrostatic potential that generates Δq. Quantities $\mathbf{J}$ and q are obtained by minimizing functionals (19) and (20) iteratively. For axi-symmetric and infinitely long geometries, $\nabla\phi$ is not required in the minimization of L_J in (19), and thence the problem is reduced to minimizing that functional [21]. We name this method as Minimum Electro Magnetic Entropy Production (MEMEP), since by minimizing (19), the entropy production is minimized [21]. In this work, we do not take surface electric charge densities into account. Then, the corresponding charge accumulates in the volume of the cells next to the surfaces. This may smear out the current density at the material interfaces. Although the variational principle above is valid for any mesh, in this article we assume uniform mesh.

Although this method allows any vector function of the $\mathbf{E}(\mathbf{J})$ relation, we use an isotropic power law for the superconductor

$$\mathbf{E}(\mathbf{J}) = E_c \left(\frac{|\mathbf{J}|}{J_c} \right)^n \frac{\mathbf{J}}{|\mathbf{J}|}, \quad (22)$$

where $E_c = 10^{-4} V/m$, J_c is the critical current and n is the power-law exponent.

C. Finite Element Method (FEM)

The FEM model is based on the H-formulation of Maxwell's equations [22], [23], where the superconductor's electrical behavior is described by (22).

D. Assumed geometry

Although all the models are suitable for complete 3D geometries, in this work we reduce the problem to 2D surfaces for simplicity. We model the soldered and striated tapes as a thin layer of 1 μm thickness with a normal conducting zone in between the superconducting regions of the same thickness. We set the resistivity between filaments (or tapes) such that the filament-to-filament resistance per unit tape length corresponds to the measurements. The models take only one cell (or element) in the thickness. The cross-sectional models additionally assume that the filaments are isolated to each other.

E. Models comparision

We compare the MEMEP and FEM models for a 4 mm wide tape of 8 mm length, 20 μm striation gap and effective normal resistivity at the gap of $2.4{\cdot}10^{-11}$ Ωm. For the superconductor, we took $J_c = 3 \cdot 10^{10}$ A/m^2 and n=30. The current density at the first peak of the AC cycle calculated by the variational principle and FEM agree to each other (see figures 2 and 3). There are small differences close to the normal metal joint because FEM uses the real gap separation of 20 μm, while MEMEP takes 49.4 μm gap and a proportionally reduced resistivity at the joint, in addition to smoothing effects due to neglecting surface charges at the interface. However, the coupling current for both methods is the same within numerical error (figure 4).

IV. Results and Discussion

A. Soldered tapes

The linear model calculations of figure 5 show that the magnitude of the current density at the peak of the applied

[2]The applied magnetic field $\mathbf{H}_a$ is related to the applied magnetic flux density $\mathbf{B}_a$ as $\mathbf{B}_a = \mu_0\mathbf{H}_a$. In this article, we refer to both as "applied magnetic field" or "applied field" for notation simplicity.

IEEE/CSC & ESAS SUPERCONDUCTIVITY NEWS FORUM (global edition), October 2015.
Invited poster presentation 3A-LS-O1.8 given at EUCAS 2015; Lyon, France, September 6 – 10, 2015.
A manuscript was submitted to *IEEE Trans. Appl. Supercond.* for possible publication.

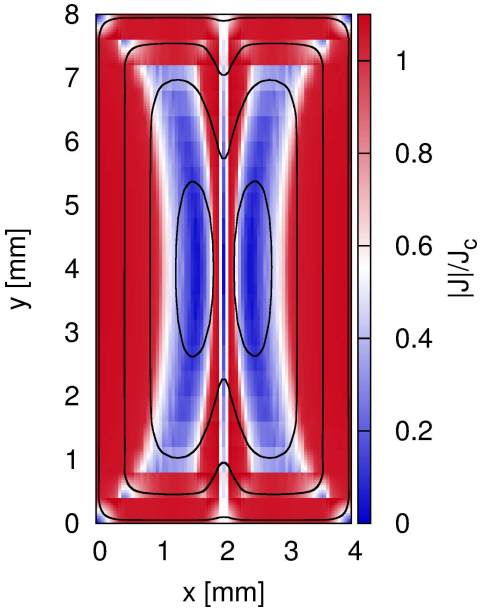

Fig. 2. Current density for the situation in section III-E calculated by MEMEP. The lines show the direction of the current flow.

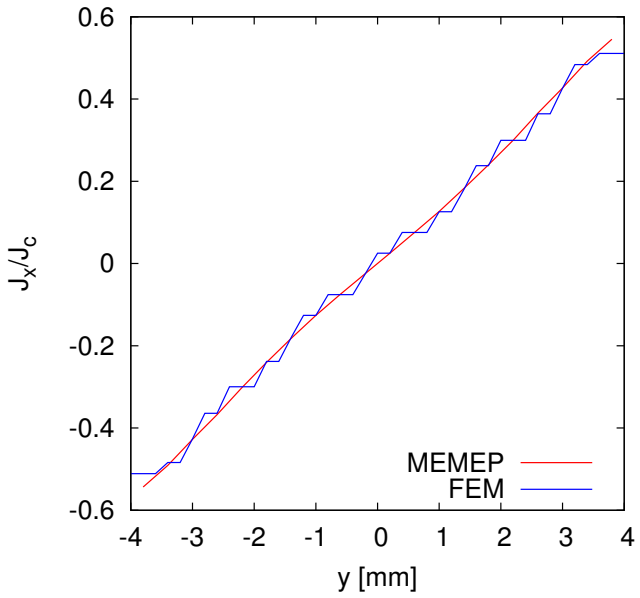

Fig. 4. The coupling current (J_x at the striation) from the MEMEP and FEM calculations agree with each other, save numerical error.

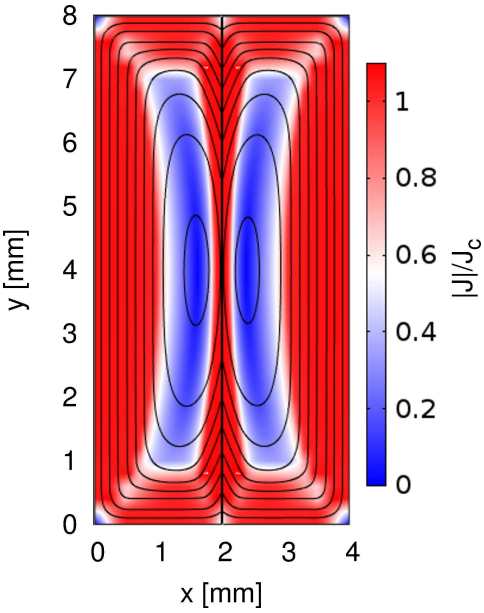

Fig. 3. Current density for the situation in section III-E calculated by FEM. The lines show the direction of the current flow.

field changes from the isolated behavior at low frequencies to full coupling at high frequencies.

The measured loss per cycle (or loss factor $\Gamma = Q/B_m^2$, where Q is the loss per cycle and sample length, and B_m is the applied field amplitude) for the isolated tapes practically does not depend on the frequency (see figures 6 and 8), and hence the loss is hysteretic. For the soldered samples, the loss presents frequency dependence, evidencing coupling loss. The peak at the frequency dependence is at 50 and 60 Hz for the 810 and 710 nΩ samples, respectively (see figure 8). The 17 % difference between samples is consistent with the $\sim$15 % difference in joint resistance. Shortening the sample from 50 to 22 mm consistently reduces the coupling loss (see figure 7).

Cross-sectional calculations of the hysteresis loss by MEMEP agree well with the measurements close to the peak of the amplitude dependence (see figure 7). For these calculations, we took constant J_c from tape measurements at self-field. The agreement is due to the fact that the magnitude of the magnetic field in the sample at self-field is similar to that for the applied magnetic field of the AC loss peak, when the sample is practically saturated with current. The higher measured loss at low fields may be caused by local J_c reduction at the tape edges or magnetic field focussing at the joint; this increases the magnetic field, and hence reduces J_c due to the actual $J_c(\mathbf{B})$ dependence. At low amplitudes, where the coupling loss dominates, the linear model agrees with the measurements (see figure 7). When adding the hysteresis loss from the cross-sectional MEMEP calculations, the total loss agrees with the measurements for magnetic field amplitudes below the peak. The agreement is worse for the short sample (22 mm length) because of the larger relative contribution of the hysteresis loss, which under-estimates the AC loss at low amplitudes, and possible finite sample effects.

The frequency dependence of the coupling loss (total loss minus hysteresis loss of the isolated sample) agrees with the calculations for the linear model (figure 8). However, the predicted peak is shifted around 17 % to higher frequencies. That may be caused by possible fluctuations of the joint resistance along the sample length, which introduces error in the measured joint resistance. The model assumptions may also cause this disagreement; the local resistivity in the superconductor is non-zero close to the joint and the currents describe 3D paths.

IEEE/CSC & ESAS SUPERCONDUCTIVITY NEWS FORUM (global edition), October 2015.
Invited poster presentation 3A-LS-O1.8 given at EUCAS 2015; Lyon, France, September 6 – 10, 2015.
A manuscript was submitted to *IEEE Trans. Appl. Supercond.* for possible publication.

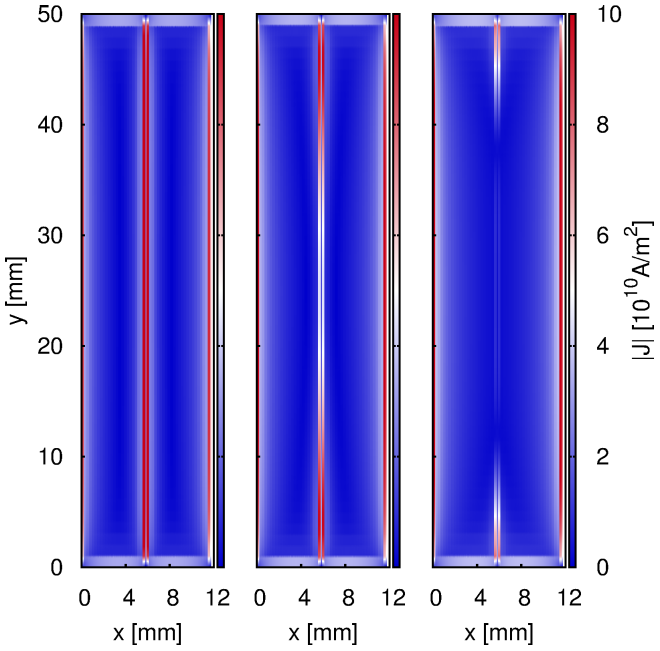

Fig. 5. Linear model results of the magnitude of the current density in soldered tapes at the peak of an AC applied magnetic field. The applied field is of 10 mT amplitude and 18, 72 and 576 Hz of frequency, from left to right. The resistance between tapes is 710 nΩ.

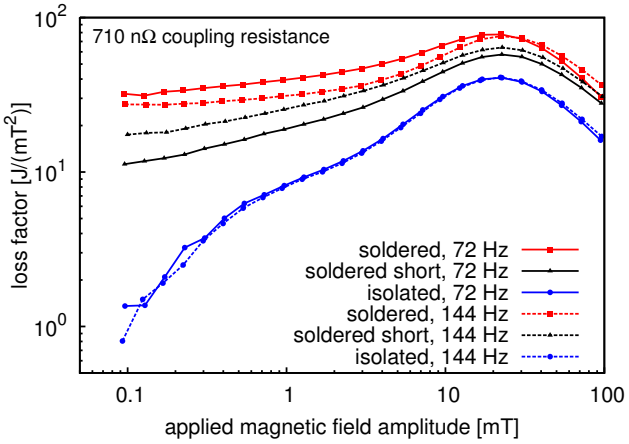

Fig. 6. Measured loss factor (Q/B_m^2, where Q is the loss per cycle and sample length and B_m is the applied field amplitude) for the soldered tapes with 710 nΩ resistance.

B. Striated tapes

Striated tapes present the same qualitative behavior as soldered tapes (figure 9).

Silver stabilized tapes present no coupling loss, since the measured loss per cycle does not present frequency dependence [5] and agrees with the cross-sectional FEM model for isolated filaments (figure 9). Again, the cross-sectional model under-estimates the loss at low amplitudes.

Copper stabilized tapes present high coupling loss at 130 Hz (figure 9) due to re-deposition of the copper after striation [17]. The linear model predicts the same order of magnitude as the measurements. When adding the hysteresis loss from the silver stabilized sample, the results agree with the measurements at

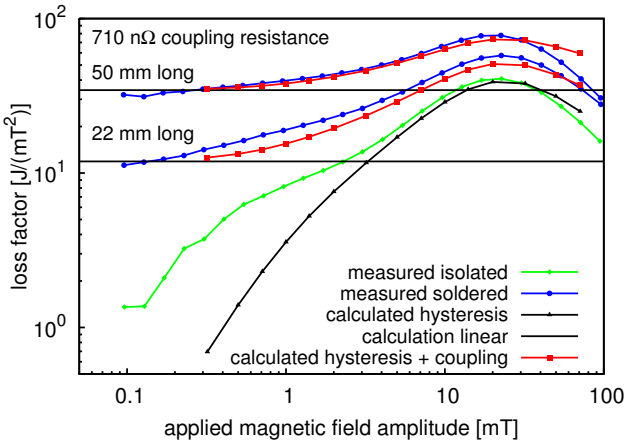

Fig. 7. The linear model ("calculation linear") agrees with the measurements for soldered tapes ("measured soldered") at low field amplitudes (72 Hz frequency). MEMEP cross-sectional calculations for constant J_c ("calculated hysteresis") agree with the measurements ("measured isolated") close to the peak of the loss factor.

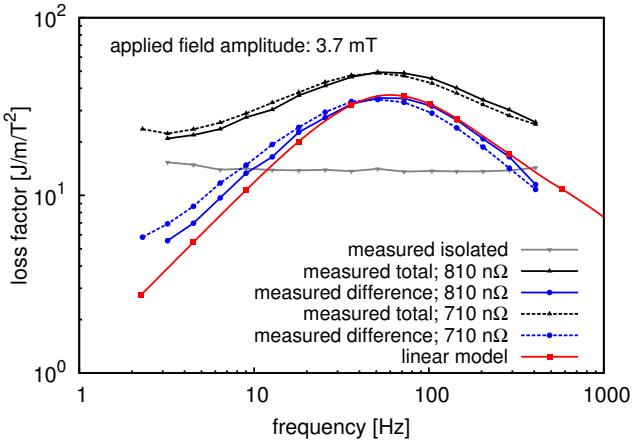

Fig. 8. The measured coupling loss, taken as the difference between that of the soldered and isolated tapes, agrees with the linear model (calculations for the 710 nΩ sample).

low amplitudes and improves the agreement for all amplitudes, except those beyond the peak. Adding the cross-sectional FEM calculations similarly improves the agreement. This suggests that the filament quality and structure of the copper stabilized tapes is the same as the silver-stabilized ones.

V. Conclusion

This article has presented a numerical and experimental study of the coupling effects in coated conductor structures like soldered tapes and striated coated conductors.

We introduced two three-dimensional numerical methods to calculate the coupling effects in superconductors. The first method, which approximates the superconductor as a material with zero resistivity, is suitable for low applied magnetic field amplitudes. The second, based on variational principles, is valid for any amplitude. We performed consistency checks by comparing to thin-strip formulas and FEM calculations, showing a good agreement.

IEEE/CSC & ESAS SUPERCONDUCTIVITY NEWS FORUM (global edition), October 2015.
Invited poster presentation 3A-LS-O1.8 given at EUCAS 2015; Lyon, France, September 6 – 10, 2015.
A manuscript was submitted to *IEEE Trans. Appl. Supercond.* for possible publication.

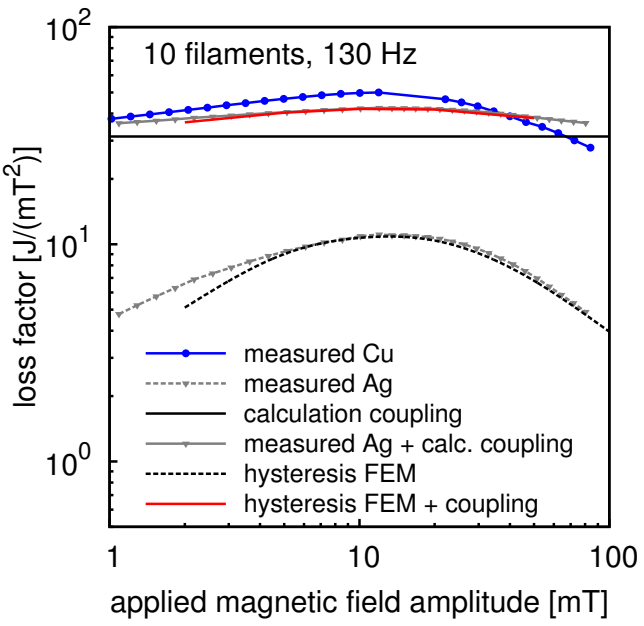

Fig. 9. AC loss for the striated tapes for the Ag-stabilized and Cu-stabilized samples. Adding the coupling loss from the linear model to the hysteresis loss agrees with the measurements.

We have found that the linear model is sufficient to predict the coupling loss at low applied field amplitudes, since the model agrees with the measurements of soldered tapes and striated coated conductors. For higher amplitudes but still below the peak of the loss factor, a fair agreement is obtained by adding the hysteresis loss from either cross-sectional models that take a realistic $E(J)$ relation into account or measurements for samples with the same superconductor geometry but no coupling effects.

The measurements for the soldered tapes suggest that soldering tapes in composite cables, such as Roebel cables, CORC cables and twisted stacks [14], [15], [24], in order to improve current sharing and stability could be used in magnets with moderate ramp rates, since the coupling loss is one order of magnitude lower than the hysteresis loss for 3 Hz or lower frequencies.

For striated tapes, the analysis of the loss measurements indicates that the superconductor in the Ag stabilized tapes is of the same quality as in the Cu stabilized tapes, the latter with a more complicated striation process.

3D linear models for the coupling loss and cross-sectional models for the hysteresis loss are sufficient to predict the total loss in coated conductor structures, except for applied field amplitudes above that of the peak of the loss factor. For that case, more sofisticated models are necessary, such as the presented 3D variational principle or FEM. Future work is intended to analyze fully 3D geometries, such as Roebel or CORC cables, as well as MgB_2 wires or other powder-in-tube conductors. For this purpose, the computing time for the 3D variational method will be optimized.

References

[1] F. Grilli, E. Pardo, A. Stenvall, D. N. Nguyen, W. Yuan, and F. Gömöry, "Computation of losses in HTS under the action of varying magnetic fields and currents," *IEEE Trans. Appl. Supercond.*, vol. 24, no. 1, p. 8200433, 2014.

[2] N. Amemiya, S. Kasai, K. Yoda, Z. Jiang, G. A. Levin, P. N. Barnes, and C. E. Oberly, "AC loss reduction of YBCO coated conductors by multifilamentary structure," *Supercond. Sci. Technol.*, vol. 17, no. 12, p. 1464, 2004.

[3] G. A. Levin, P. N. Barnes, N. Amemiya, S. Kasai, K. Yoda, and Z. Jiang, "Magnetization losses in multifilament coated superconductors," *Appl. Phys. Lett.*, vol. 86, no. 7, p. 072509, 2005.

[4] G. Levin, J. Murphy, T. J. Haugan, J. Souc, J. Kovac, and P. Kovac, "AC losses of copper stabilized multifilament YBCO coated conductors," *IEEE Trans. Appl. Supercond.*, vol. 23, no. 3, p. 6600604, 2013.

[5] E. Demencik, F. Grilli, A. Kario, R. Nast, A. Jung, M. Vojenciak, J. Scheiter, and W. Goldacker, "AC magnetization loss and transverse resistivity of striated YBCO coated conductors," *IEEE Trans. Appl. Supercond.*, vol. 25, no. 3, pp. 1–5, 2015.

[6] N. Amemiya, F. Kimura, and T. Ito, "Total AC loss in twisted multifilamentary coated conductors carrying AC transport current in AC transverse magnetic field," *IEEE Trans. Appl. Supercond.*, vol. 17, no. 2, pp. 3183–3186, 2007.

[7] J. Šouc, F. Gömöry, J. Kováč, R. Nast, A. Jung, M. Vojenčiak, F. Grilli, and W. Goldacker, "Low AC loss cable produced from transposed striated CC tapes," *Supercond. Sci. Technol.*, vol. 26, no. 7, p. 075020, 2013.

[8] F. Grilli, M. Costa Bouzo, Y. Yang, C. Beduz, and B. Dutoit, "Finite element method analysis of the coupling effect between superconducting filaments of different aspect ratio," *Supercond. Sci. Technol.*, vol. 16, no. 10, p. 1228, 2003.

[9] M. C. Bouzo, F. Grilli, and Y. Yang, "Modelling of coupling between superconductors of finite length using an integral formulation," *Supercond. Sci. Technol.*, vol. 17, no. 10, p. 1103, 2004.

[10] S. Kasai and N. Amemiya, "Numerical analysis of magnetization loss in finite-length multifilamentary YBCO coated conductors," *IEEE Trans. Appl. Supercond.*, vol. 15, no. 2, pp. 2855–2858, 2005.

[11] L. Prigozhin, "Solution of thin film magnetization problems in type-II superconductivity," *J. Comput. Phys.*, vol. 144, no. 1, pp. 180–193, 1998.

[12] J. W. Barrett and L. Prigozhin, "Electric field formulation for thin film magnetization problems," *Supercond. Sci. Technol.*, vol. 25, no. 10, p. 104002, 2012.

[13] C. Navau, A. Sanchez, N. Del-Valle, and D. X. Chen, "Alternating current susceptibility calculations for thin-film superconductors with regions of different critical-current densities," *J. Appl. Phys.*, vol. 103, p. 113907, 2008.

[14] W. Goldacker, F. Grilli, E. Pardo, A. Kario, S. I. Schlachter, and M. Vojenčiak, "Roebel cables from REBCO coated conductors: a one-century-old concept for the superconductivity of the future," *Supercond. Sci. Technol.*, vol. 27, no. 9, p. 093001, 2014.

[15] D. C. Van der Laan, "$YBa_2Cu_3O_{7-\delta}$ coated conductor cabling for low ac-loss and high-field magnet applications," *Supercond. Sci. Technol.*, vol. 22, no. 6, p. 065013, 2009.

[16] SuperPower, Inc. http://www.superpower-inc.com/.

[17] A. Kario, R. Nast, A. Jung, B. Ringsdorf, J. Scheiter, E. Demencik, A. Godfrin, F. Grilli, A. Molodyk, A. Mankevich, and W. Goldacker, "Effectiveness of the laser striation for AC loss reduction in SuperOx coated conductors," http://snf.ieeecsc.org/abstracts/stp453-effectiveness-laser-striation-ac-loss-reduction-superox-coated-conductors.

[18] J. Šouc, F. Gömöry, and M. Vojenčiak, "Calibration free method for measurement of the ac magnetization loss," *Supercond. Sci. Technol.*, vol. 18, no. 5, p. 592, 2005.

[19] J. Kováč, J. Šouc, P. Kováč, I. Hušek, and F. Gömöry, "Experimental study of magnetization AC loss in MgB_2 wires and cables with non-magnetic sheath," *Physica C*, vol. 495, pp. 182–186, 2013.

[20] J. Kováč, J. Šouc, P. Kováč, and I. Hušek, "Magnetization AC losses in MgB_2 wires made by IMD process," *Supercond. Sci. Technol.*, vol. 28, no. 1, p. 015013, 2015.

[21] E. Pardo, J. Šouc, and L. Frolek, "Electromagnetic modelling of superconductors with a smooth current-voltage relation: variational principle and coils from a few turns to large magnets," *Supercond. Sci. Technol.*, vol. 28, p. 044003, 2015.

[22] R. Brambilla, F. Grilli, and L. Martini, "Development of an edge-element model for AC loss computation of high-temperature superconductors," *Supercond. Sci. Technol.*, vol. 20, no. 1, pp. 16–24, 2007.

IEEE/CSC & ESAS SUPERCONDUCTIVITY NEWS FORUM (global edition), October 2015.
Invited poster presentation 3A-LS-O1.8 given at EUCAS 2015; Lyon, France, September 6 – 10, 2015.
A manuscript was submitted to *IEEE Trans. Appl. Supercond.* for possible publication.

[23] F. Grilli, R. Brambilla, F. Sirois, A. Stenvall, and S. Memiaghe, "Development of a three-dimensional finite-element model for high-temperature superconductors based on the H-formulation," *Cryogenics*, vol. 53, pp. 142–147, 2013.
[24] M. Takayasu, L. Chiesa, L. Bromberg, and J. V. Minervini, "HTS twisted stacked-tape cable conductor," *Supercond. Sci. Technol.*, vol. 25, no. 1, p. 014011, 2012.